

Effects of variable thermal diffusivity on the structure of convection

O.V. Shcheritsa¹ · A.V. Getling² ·
O.S. Mazhorova¹

© Springer

Abstract The multiscale flow structure in the solar convection zone, i.e., the coexistence of such features as the granules, mesogranules, supergranules and giant cells, has not yet been properly understood. Here, the possible role of one physical factor – variations in the thermal diffusivity – in the formation of a multiscale convection structure is investigated. Thermal convection in a plane horizontal fluid layer is numerically simulated. The temperature dependence of thermal diffusivity is chosen so as to produce a sharp kink in the static temperature profile near the upper layer boundary. As a result, the magnitude of the (negative) static temperature gradient $[dT_s/dz]$, being small over the most part of the layer thickness, reaches large values in a thin boundary sublayer. To identify the structures on different scales, we apply a smoothing procedure, computational-homology techniques and spectral processing to the temperature field. The flow is found to be a superposition of three cellular structures with three different characteristic scales. The largest (first-scale) convection cells, with central upflows, fill the whole layer thickness; most of these cells are divided by “bridges”, or “isthmuses” into a few smaller (second-scale) ones, which are localised in the upper portion of the layer; finally, there are numerous tiny (third-scale) features that dot the horizontal sections of the layer located near its upper boundary and exhibit a tendency of gathering in the intercellular lanes of the first-scale cells. The third-scale cellular structures are advected by the first-scale and second-scale convective flows. The spatial spectrum of the flow does not

✉ A.V. Getling
a.getling@mail.ru
O.V. Shcheritsa
shchery@mail.ru
O.S. Mazhorova
olgamazhor@mail.ru

¹ Keldysh Institute of Applied Mathematics, Moscow, 125047 Russia

² Skobeltsyn Institute of Nuclear Physics, Lomonosov Moscow State University, Moscow, 119991 Russia

directly indicate the presence of the second-scale and third-scale structures; however, they can be selected by using the above-mentioned processing techniques. On the whole, the simulated flow pattern qualitatively resembles that observed on the Sun.

Keywords: Convection; Variable thermal diffusivity; Flow scales

1. Introduction

This study was motivated by the necessity of comprehending the physical factors responsible for the complex spatial structure of solar convection. The magnetic fields in the solar convection zone are dynamically coupled with motions, and the formation of convection patterns is of paramount importance to the dynamics of magnetic fields and, therefore, to the processes of solar activity. As is well known, cellular structures of at least three or four scales can be identified with certainty on the solar surface and attributed to the phenomenon of thermal convection, viz., granules, mesogranules (whose existence as a physical entity is debatable), supergranules and giant cells (see, in particular, Nordlund, Stein, and Asplund, 2009; Rieutord and Rincon, 2010, and references therein). They differ widely in their scale. Moreover, Abramenko *et al.* (2012) reported the detection of mini-granular structures with spatial scales below 600 km and a broad size distribution. Smaller cells are transferred by the motions associated with the larger scales. This multiscale structure (or scale splitting) is an important feature of solar convection, which should be taken into account in studying the dynamics of magnetic fields. It has not yet received a convincing explanation, and an adequate hydrodynamic description must be given to both the spatial structure of the flows and the factors responsible for its development.

The discreteness of the scale distribution of solar convection structures can be noted based on the analyses of granulation images (see, e.g., Simon *et al.*, 1994) and on Doppler measurements, which detect supergranulation (Leighton, Noyes, and Simon, 1962; Simon and Leighton, 1964), mesogranulation (November *et al.*, 1981) and giant cells (Beck, Duvall, and Scherrer, 1998; Beck *et al.*, 1998); it can also be inferred from the field of horizontal photospheric velocities. However, the power spectra of the velocity field seem to exhibit only two peaks corresponding to granulation and supergranulation (see, e.g., Hathaway *et al.*, 2000).

Likely, the power spectra are not sufficiently informative in terms of detecting all really present cellular flows. In particular, Shine, Simon, and Hurlburt (2000) found mesogranules in a size range of 4–7 Mm using local correlation tracking (LCT), and Lawrence, Cadavid, and Ruzmaikin (2001) employed a wavelet technique to reveal 4-Mm-large cells. The existence of giant cells was evidenced by tracking the motion of supergranules (Hathaway, Upton, and Colegrove, 2013). An LCT-based cork-motion technique very clearly visualises both supergranules and mesogranules (Getling and Buchnev, 2010). A further discussion of the pros and cons concerning the existence of mesogranules is given by Rieutord and Rincon (2010).

In contrast, some “realistic” (or, according to Schüssler, 2013, “comprehensive”) simulations based on the *MURaM* code (Vögler *et al.*, 2005) demonstrate

a gradual increase in the characteristic scale of convection with depth (Schüssler, 2014). According to such simulations, the surface velocity field does not demonstrate any multiscale structure, and only granular-sized cells are clearly noticeable in the computed patterns. Larger-scale structures cannot be detected in the surface velocity field; at most, they may be too weak to manifest themselves in advecting small-scale cells, as observed on the solar surface. This suggests that some factors responsible, e.g., for supergranulation are not taken into account in the formulation of the problem.

Our aim is to investigate the role of some factors that can produce the static temperature profile of a particular shape in the convection layer, thus giving rise to a multiscale structure of the velocity field. Specifically, we are interested in the effects of temperature-dependent thermal diffusivity. We assume this quantity to be represented by a high-degree polynomial in temperature, so that the static temperature gradient is small in the bulk of the layer but makes a jump to high absolute values in a thin sublayer near the top boundary of the layer. We regard such a jump as a model representation of a partial-ionisation layer in the solar convection zone, where the enhanced specific heat reduces the adiabatic thermal gradient and the enhanced opacity increases the radiative thermal gradient. The convective instability of this layer is therefore especially high (Simon and Leighton, 1964; November *et al.*, 1981); the most pronounced jump of the vertical entropy gradient due to partial ionisation is present at depths of order 1 Mm below the solar photosphere.

It should be noted that the particularities of the behaviour of thermal diffusivity and those of the stratification do not exhaust the factors that can give rise to scale splitting. Hydrodynamic instabilities of larger-scale flows can produce secondary, smaller-scale flows. At the same time, according to Brummell, Cattaneo, and Toomre (1995), self-organisation processes (inverse energy cascades) can give rise to coherent structures. Cattaneo, Lenz, and Weiss (2001) note that mesogranules can develop as a result of the collective interaction between granules and leave the effects of stratifications beyond the scope of their study.

Linear problems of convective stability in layers with similar static temperature profiles were considered by Getling (1975, 1980). In the framework of the models, indirect evidence for possible scale splitting was found. However, the development of small-scale convective motions near the surface of the layer requires very sharp gradient jumps and very thin high-gradient sublayers. These expectations were partially substantiated by two-dimensional nonlinear numerical simulations (Getling and Tikhomolov, 2007). Recently, we studied the two-dimensional problem more extensively, see Getling, Mazhorova, and Shcheritsa (2013) and Shcheritsa, Getling, and Mazhorova (2015) (hereinafter, Paper I).

Here, we present the results of our simulations of three-dimensional convection under conditions similar to those assumed in Paper I (a special form of the temperature dependence of thermal diffusivity, which ensures a sharp kink in the static temperature profile). We shall demonstrate that, even in the framework of our simple model based on an extended Boussinesq approximation, variable thermal diffusivity can be demonstrated to be a possible producer of a multiscale flow in which at least three cell types are present.

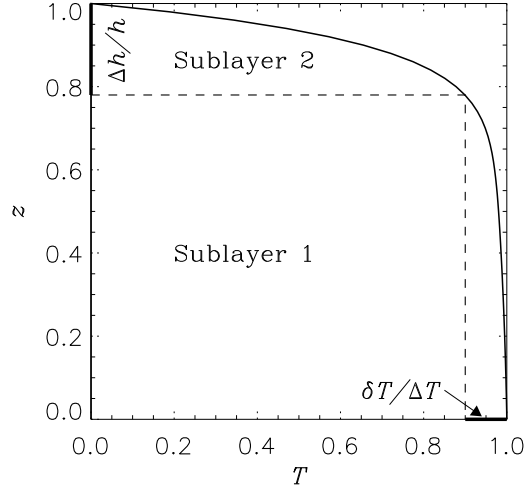


Figure 1. Static temperature profile due to the $\chi(T)$ dependence specified by (1).

2. Formulation of the problem and numerical technique

We consider a rectangular domain $[0, L_x] \times [0, L_y] \times [0, h]$ of a plane horizontal layer of a viscous, incompressible fluid (in our computations described here, $L_x = L_y = 15h$). Assume the bottom and the top boundary of the layer to be perfect thermal conductors, whose temperatures are maintained constant and equal to $T_{\text{bot}} = \Delta T > 0$ and $T_{\text{top}} = 0$, respectively. Also assume the sidewalls of the region to be thermally insulated. We specify the no-slip impermeability conditions at the bottom and side boundaries of the region. In the simulation that will be described here, the top boundary is also assumed to be rigid. We plan to investigate the case of a free-slip upper boundary at a later time.

We choose the temperature dependence of thermal diffusivity in the form

$$\chi(T) = 1 + 5T + 600T^{10}. \quad (1)$$

This means that the static temperature varies little (by $\delta T \ll \Delta T$) across the main portion of the layer, of thickness $h - \Delta h$, $\Delta h \ll h$ (Sublayer 1), while the most part of the temperature difference, $\Delta T - \delta T$, corresponds to Sublayer 2 with a small thickness Δh , near the upper surface (Fig. 1). The kink near $z = h - \Delta h$ in the temperature profile specified in this way qualitatively resembles the transition from the bulk of the solar convection zone, where the stratification is weakly superadiabatic, to the overlying strongly unstable layer with a depth of order 1 Mm.

We use an extended Boussinesq approximation, which admits thermal-diffusivity variations (see, e.g., Getling, 1998, for a discussion of different versions of this approximation). If the layer thickness h is used as the unit length, ΔT as the unit temperature and the characteristic time of viscous momentum transport

$[\tau_\nu = h^2/\nu]$ as the unit time (ν being the kinematic viscosity), the governing equations assume the following dimensionless form:

$$\frac{\partial \mathbf{v}}{\partial t} + (\mathbf{v} \cdot \nabla) \mathbf{v} = -\nabla \varpi + \hat{\mathbf{z}} \frac{R}{P} (T - T_s) + \nabla^2 \mathbf{v}, \quad (2)$$

$$\frac{\partial T}{\partial t} + \mathbf{v} \cdot \nabla T = \frac{1}{P} \nabla \cdot \frac{\chi(T)}{\chi(T_{\text{top}})} \nabla T, \quad (3)$$

$$\nabla \cdot \mathbf{v} = 0. \quad (4)$$

Here, t is the time, x, y, z are Cartesian coordinates, \mathbf{v} is the velocity vector, ϖ is the pressure, T is the temperature, $T_s(z)$ is the static temperature distribution, $\hat{\mathbf{z}} = (0, 0, 1)$ and

$$R = \frac{\alpha g \Delta T h^3}{\nu \chi(T_{\text{top}})} \quad \text{and} \quad P = \frac{\nu}{\chi(T_{\text{top}})}$$

are the Rayleigh and Prandtl numbers, α being the volumetric coefficient of thermal expansion of the fluid and g the gravitational acceleration.

To solve the Navier–Stokes equations, we use a modification of the known semi-implicit method of a predictor–corrector class based on staggered grids. In essence, it replaces the incompressibility equation with a Poisson equation for pressure. First, a predictor for velocity is calculated from the equation of motion. Next, a pressure corrector is found, which is used to correct the velocity field so as to ensure incompressibility. The spatial approximation of the equations is chosen based on the conservativeness requirement; it has a second-order approximation inside the domain and a first-order approximation at the boundary.

Initially, the fluid is motionless. The flow originates from a random temperature perturbation of the temperature profile introduced at a certain height inside Sublayer 2, which is convectively most unstable.

3. Simulation results

3.1. Qualitative description

We consider here a representative computational run for which $R = 1.5 \times 10^8 \approx 37.5 R_c$, where the critical Rayleigh number was determined in the course of simulations to be $R_c \approx 4 \times 10^6$, and $P = 1$. The flow starts developing in Sublayer 2 and gradually involves the whole layer in motion.

Figure 2a–c shows the distributions of the vertical velocity component over horizontal sections of the computational domain at three levels. The clearly visible large cellular structures exhibit, for some time, a tendency of increasing their sizes, with slight deformations and drift. They gradually fill the entire depth of the layer, and their growth virtually terminates by times $t \approx 0.16$. We designate these structures as the *first-scale* cells. A well-developed convection pattern with diverse structural features forms by $t \approx 0.26$. As this pattern has been established, the areas of large velocity-field structures in the sections located near the upper layer boundary appear to be peppered with a multitude of

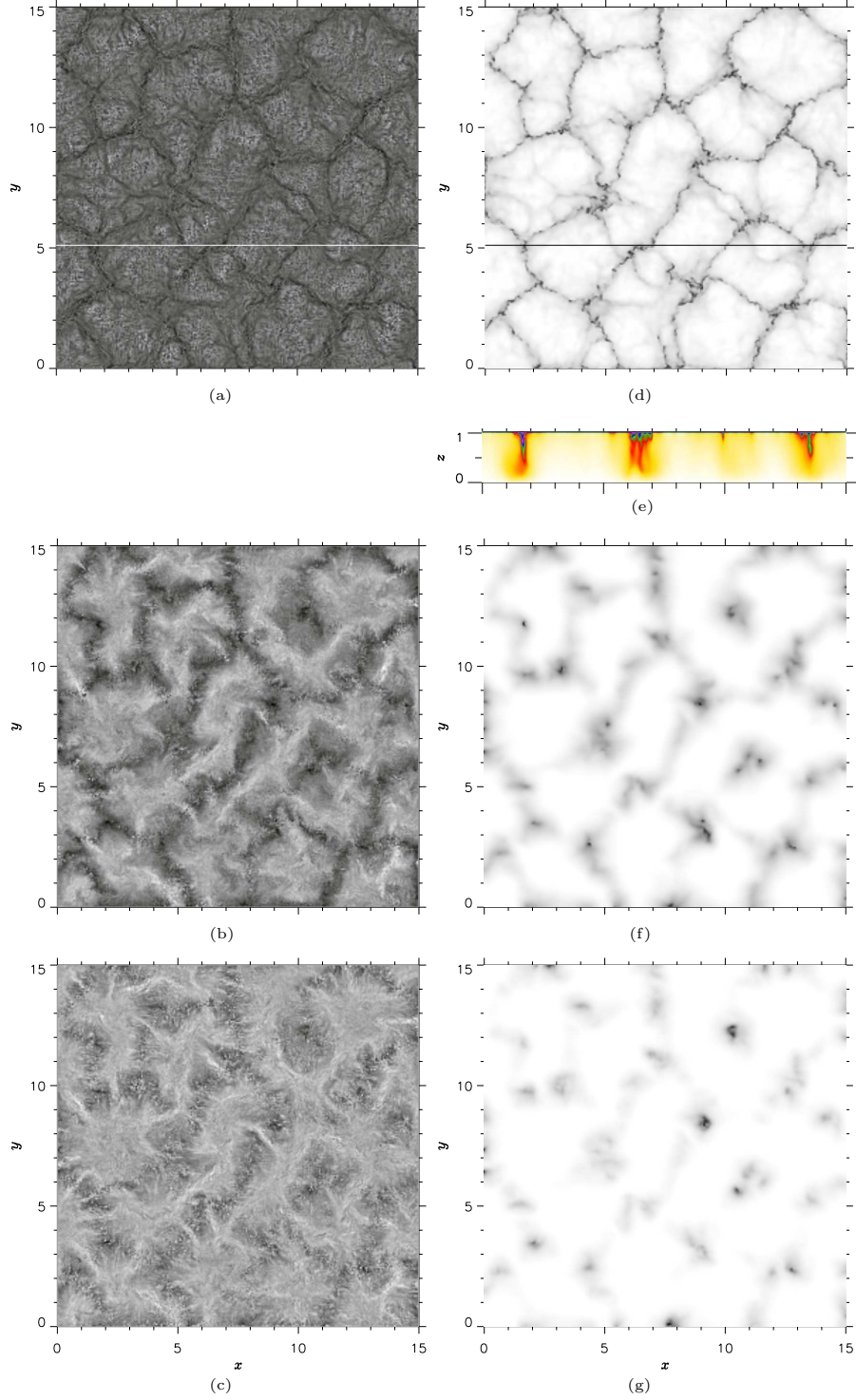


Figure 2. (a)–(c) Vertical velocity component at $z = 0.97, 0.323, 0.161$, with variation ranges $[-0.44, 0.64]$, $[-0.75, 0.60]$, $[-0.80, 0.49]$, respectively; (d), (f), (g) temperature field at the same levels with variation ranges $[0.01, 0.99]$, $[0.45, 0.99]$, $[0.49, 1.00]$, respectively; the greyscale for either variable is everywhere normalised to the corresponding range; (e) temperature distribution in the vertical section $y = 5.11$ marked in (a), (b) with the horizontal lines (the z -scale is exaggerated with respect to the x -scale to clarify the structure of the descending plumes; high thermal conductivity in deep layers prevents the cold plumes from reaching the bottom surface).

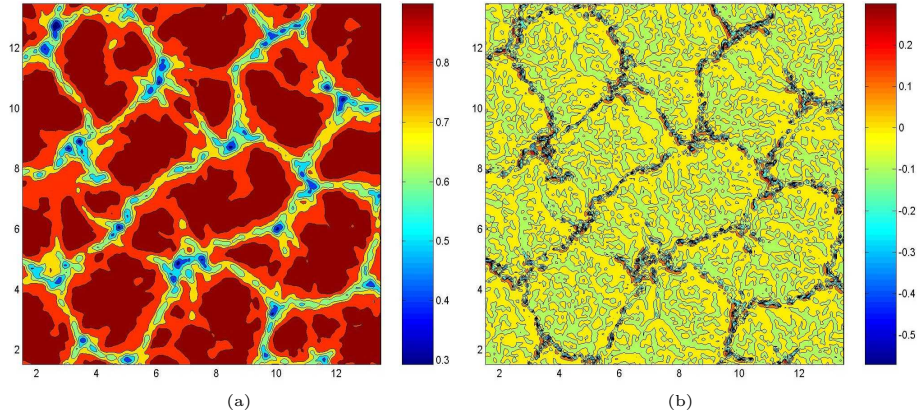


Figure 3. Processing of the temperature field at $z = 0.97$ with a moving-average filter: (a) long-wavelength component, averaging result; (b) short-wavelength component obtained by subtracting the average from the original field.

small features, which move following their own laws and approaching the borders of the large structures (Fig. 2a). The small structures emerge over the entire area of a first-scale cell, and small-scale cells can be identified in their pattern (see Section 3.2). We assign them to a *third scale*. Cells of an intermediate *second scale* can also be detected; they will become even more clear-cut upon applying a spectral processing (Section 3.4). The abundance and movability of the fine features produce the impression of a “seething” process, which involves the entire horizontal section. The generation centre of this process cannot be located. A similar pattern can be observed in the temperature field (Fig. 2d, f, g), where the same structures can be identified.

The borders of the first-scale structures coincide in their location with the strongest downflows. The temperature variations over the horizontal section $z = 0.97$ (see Fig. 2d) are within the range $T_{\max} - T_{\min} = 0.98$. Not every cold plume arrives at the bottom of the layer because of the high thermal diffusivity (Fig. 2e). The flow near the bottom surface is not so diverse: there are only several isolated plumes, which are relatively far apart, while small-scale structures considerably differing from the corresponding large structures in their temperatures and velocities are observed only in the upper portion of the layer.

3.2. Smoothing the field and singling out the small-scale features

To single out different flow scales, we apply a moving-average filter to the temperature field. Figure 3a shows the result of averaging with a Gaussian filter; Fig. 3b, the result of subtracting the average from the original flow pattern. The averaged, long-wavelength component of the flow is basically represented by the largest (first-scale) structures; however, the averaging procedure also reveals some “bridges”, or “isthmuses” (shown in bright red), which were not so noticeable in the original flow map. They reflect the presence of structures on an intermediate, second scale. These features will become especially pronounced

upon applying spectral and computational-homology techniques to processing the flow pattern (see Fig. 11 in Section 3.4 and Fig. 6 in Section 3.3).

The subtraction of the average from the flow pattern yields the short-wavelength component of the flow (Fig. 3b). The small-scale structures fill the whole horizontal section, their density being higher near the borders of the large structures. The periphery of the large (primary) structures is formed by the strongest down-drafts, which run through the whole layer, from top to bottom. However, there are plumes permeating only part of the layer depth (Fig. 2e), to the levels where they become smeared due to the high thermal conductivity.

3.3. Computational homology

As already noted, the third-scale structures fill the whole horizontal section $z = \text{const}$ in the upper portion of the layer (Figs. 2a, d). In view of this, to analyse the geometric properties of complex structures (patterns) emerging in the strongly time-dependent convective flow, we used techniques developed in the *Computational-Homology Project* (*CHomP*; see Mischaikow *et al.*, 2002; Kaczynski, Mischaikow, and Mrozek, 2003). To isolate particular features in the flow pattern, it is necessary to specify, using some criterion, a topological space to which these features belong. As such a criterion, we choose the departures of the temperature from its average over a horizontal section and construct two topological spaces (areas) where the temperature is higher or lower than this average. We shall call them the hot and cold areas, respectively.

We describe the flow structure using topological invariants known as Betti numbers. The zeroth Betti number $[\beta_0]$ is the number of connected components of the given region. The first Betti number $[\beta_1]$ is the number of independent cycles other than the boundary of the region. The notion of the independent cycle is illustrated in Fig. 4. The red contour (or cycle) can be constricted into a point via a continuous deformation. The blue cycle, which can be constricted only to the white region, is termed an *independent cycle*. In a two-dimensional geometry, independent cycles are in essence holes in the region. In our example, the Betti numbers are $\beta_0 = 1$, $\beta_1 = 1$ for the grey region and $\beta_0 = 1$, $\beta_1 = 0$ for the white region.

We determine the topological invariants separately for hot and cold areas, since the information for only one sort is insufficient to judge the flow structure. Let us first comprehend what this technique should yield for ideal, quite regular convection structures, viz., two-dimensional straight rolls and three-dimensional hexagonal cells. Consider an arbitrary chosen horizontal section of a system of rolls (Fig. 5a). In downflows, the fluid temperature is below the average, and we fill the downflow areas with black. Conversely, let the upflow areas, which have temperature above the average, be filled with white. Assume that the flow under study consists of a number of rolls, with alternating upflow and downflows. In this case, we shall have alternating white and black bands in a horizontal section, their widths varying with height. Let us evaluate the Betti numbers for this case. The number of hot and cold bands either are equal or differ by 1, depending on the choice of the domain to be considered (for simplicity, we consider a rectangular domain and assume that the rolls are parallel to its side

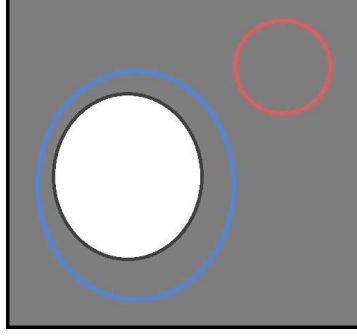


Figure 4. Illustration to the notions used in computational homology: the red contour is a cycle; the blue one, an independent cycle.

boundary). Therefore, typically, $\beta_0^h = \beta_0^c \pm 1$ and $\beta_1^{h,c} = 0$, where the superscripts h and c refer to the hot and cold regions. If the pattern is not ideal, and the rolls have imperfections (there are, e.g., smaller-scale convection cells superposed on the basic flow), the above relationships become less strict: $\beta_0^h \sim \beta_0^c$, $\beta_1^{h,c} \ll \beta_0^{h,c}$. Therefore, if such relationships hold for the flow pattern, we can conclude that the flow is of a roll type.

Now assume that the flow pattern is formed by three-dimensional, e.g., hexagonal, convection cells (Fig. 5b). If the hot upflows are located in the central parts of the cells and the cold downflows in their peripheral parts, β_0^h for a perfect pattern should be large, equal to the number of cells, and no holes should be present in the hot regions: $\beta_1^h = 0$. Accordingly, there should be only one cold region, which implies $\beta_0^c = 1$, and the number of holes in it should be equal to the number of cells, so that $\beta_1^c = \beta_0^h \gg 1$. For a nonideal pattern, apart from the fact that the network of the intercellular downflow lanes may have a more complex structure, hot inclusions may be present in this cold region and cold inclusions in the hot upflows inside the cells. They will reflect smaller-scale cells against the background of the basic-scale convection. In this case, the Betti-number relationships obviously assume the softer form $\beta_1^c \approx \beta_0^h$, $\beta_0^h \gg \beta_1^h$, $\beta_0^c \ll \beta_1^c$. Therefore, if we find that the Betti numbers are related in such way, we can suggest that the flow consists of cells with central upflows. Similarly, the relationships $\beta_0^c \approx \beta_1^h$, $\beta_1^h \gg \beta_0^h$, $\beta_1^c \ll \beta_0^c$ will be indicative of cells with central downflows. However, as we shall see now, a visual control will nevertheless be needed.

For our problem, we calculate β_0 and β_1 for hot and cold regions employing the *CHomP* code (Mischaikow *et al.*, 2002). The hot and cold areas in three horizontal planes at various z are shown in Fig. 6. Observe that the network of heavy black areas exactly corresponds to the peripheral regions of the large structures formed by the strongest downdrafts, which run through the whole layer depth (cf. Figs. 2a, d). As noted in Section 3.2, there are also plumes that do not reach the bottom surface of the layer (Fig. 2e). The interiors of the large structures are mainly white, with small black islands; the black “bridges”, or

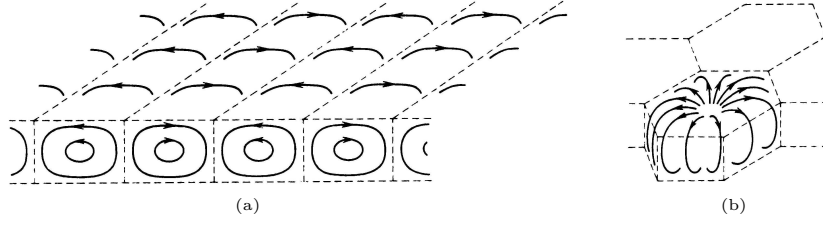


Figure 5. Schematic representation of two types of regular convection cells: (a) convection rolls, $\beta_0^h \sim \beta_0^c$, $\beta_1^{h,c} \ll \beta_0^{h,c}$; (b) hexagonal convection cells with upflows in their central parts, $\beta_0^h \gg \beta_1^h$, $\beta_0^c \ll \beta_1^c$.

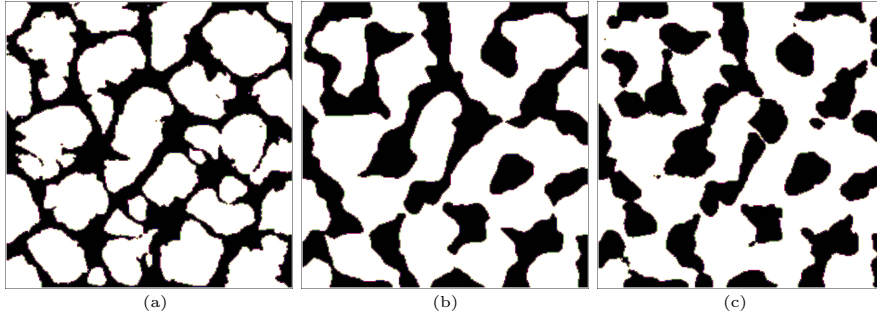


Figure 6. Flow pattern prepared for processing using the computational-homology techniques. The black areas are colder than the average and white areas are warmer: (a) $z = 0.97$, $\beta_0^h = 55$, $\beta_1^h = 34$, $\beta_0^c = 29$, $\beta_1^c = 49$; (b) $z = 0.38$, $\beta_0^h = 8$, $\beta_1^h = 2$, $\beta_0^c = 9$, $\beta_1^c = 0$; (c) $z = 0.1$, $\beta_0^h = 2$, $\beta_1^h = 12$, $\beta_0^c = 24$, $\beta_1^c = 4$.

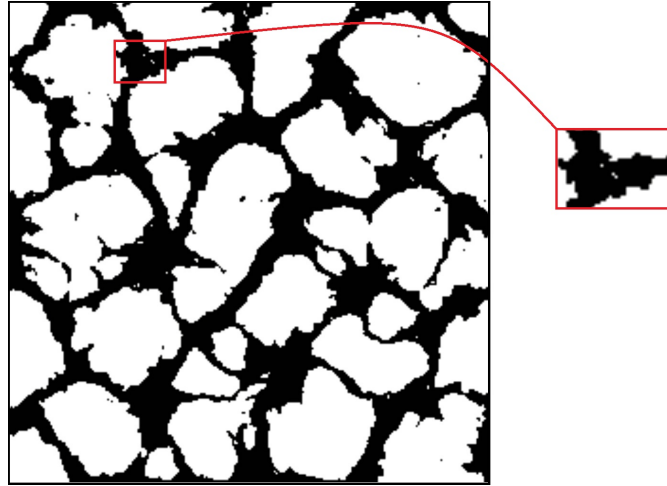


Figure 7. Cold and hot areas, $z = 0.97$, $\beta_0^h = 55$, $\beta_1^h = 34$, $\beta_0^c = 29$, $\beta_1^c = 49$.

“isthmuses”, that can be seen at $z = 0.97$ (Fig. 6a) but cannot at $z = 0.38$ (Fig. 6b) correspond precisely to these, not so strong, plumes. Even a visual inspection of Fig. 6 indicates that black islands are present only in horizontal sections through the upper portion of the layer. Thus, small-scale structures are localised only in the upper part of the layer, being indistinguishable in deep layers (see Figs 6b for $z = 0.38$ and 6c for $z = 0.1$).

Based on the above-presented considerations for elementary flows structures, we could conclude that the computed flow should resemble cells with central upflows (l-cells) at $z = 0.97$, rolls at $z = 0.38$ and cells with central downflows (g-cells) at $z = 0.1$. However, the flow pattern at $z = 0.1$ does not appear as a cellular structure. The procedure of constructing cold and hot areas is formal; really, the temperature differences in this section are small, $T_{\max} - T_{\min} = 0.09$. In other words, our technique is similar to employing a magnifying glass to examine an apparently straight line, which is actually not straight. The obtained black spots merely reflect cold descending plumes, which are rapidly heated near the bottom because of the high thermal conductivity. Therefore, in contrast to suggestions based on the Betti numbers, no multiscale flow can be observed near the bottom but there are only isolated cold plumes reaching the bottom; their interaction is very weak (see Fig. 2e).

The section $z = 0.97$ is of particular interest, since very large Betti numbers were found for it. Although only one connected region and several islands can be revealed visually, the software package for the calculation of the Betti numbers yields $\beta_0^c = 29$ for connected colds areas and $\beta_0^h = 55$, i.e., almost twice as many hot ones. To understand why so many connected areas were found, a “magnifying glass” proved to be needed (Fig. 7). It turned out that there are small white islands, or spots, located inside black areas. Thus, warm regions exhibiting a tendency toward ascending motion are present inside the sinking plumes. The overall temperature difference in this section is large, $T_{\max} - T_{\min} = 0.97$. As can be judged by β_0^c and β_0^h , there are many such areas, and such a relation between the Betti number may be indicative of the presence of a second flow scale. Note that, except black islands inside hotter regions, there are narrow black bridges, which, however, are virtually unnoticeable in the flow pattern (Fig. 2).

The black islands inside the large white areas (Fig. 7, right) correspond to small-scale structures. They are numerous, and their amount can be estimated using computational-homology techniques for a three-dimensional region. In this case, one more Betti number $[\beta_2]$ can be introduced. It is equal to the number of “holes” in the region. In our three-dimensional problem, $\beta_0^{c(3D)} = 107$, $\beta_1^{c(3D)} = 28$, $\beta_2^{c(3D)} = 0$, $\beta_0^{h(3D)} = 51$, $\beta_1^{h(3D)} = 26$, $\beta_2^{h(3D)} = 3$. We expected to find large $\beta_2^{h(3D)}$ and $\beta_2^{c(3D)}$. However, the result of our calculations proved to be different: since the small-scale structures are localised in a thin upper portion of the layer, the code calculating the Betti numbers interpreted these structures (black islands) as connected areas and included their number in $\beta_0^{h(3D)}$ and $\beta_0^{c(3D)}$.

Let us give an illustrating example. Consider a sphere inside a spherical shell (Fig. 8). The Betti numbers for the grey region are $\beta_0^{(3D)} = 2$, $\beta_1^{(3D)} = 0$, $\beta_2^{(3D)} = 1$, i.e., we have two connected regions – the inner sphere and the outer

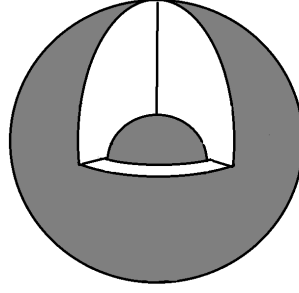


Figure 8. Illustration to the processing of three-dimensional fields with the *CHomP* code (see text).

spherical shell; no independent cycles, since all of them can be constricted to a point via a continuous deformation; and one “hole” – the gap between the sphere and the shell. If we consider the same geometry but with a part of the shell cut off, we shall obtain a cup with a sphere inside. In this case, the Betti numbers become $\beta_0^{(3D)} = 2$, $\beta_1^{(3D)} = 0$, $\beta_2^{(3D)} = 0$, since the cup and the sphere remain connected regions but the gap is no longer a hole.

In our study, we expected to find many small connected regions (the third scale) inside the shells (the first scale); these shells, formed by downdrafts, can be seen in Fig. 6. However, as in the above-described example, the shells are not closed, and these islands prove to be counted in the zeroth Betti number (the number of connected regions) rather than the second one. The *CHomP* code computing the Betti numbers yields $\beta_0^{c(3D)} = 107$, or almost twice as many as for two-dimensional sections. It is this fact that should be regarded as evidence for the existence of numerous small-scale structures.

3.4. Spectral properties of the flow

Now, to comprehend how the flow spectrum reflects the presence of the three convection scales revealed in our simulations, we analyse the flow structure using spectral techniques. Figure 9 represents the spectrum of the temperature field shown in Fig. 2d. In the low-wavelength range corresponding to wavenumbers $1.8 < k < 2$, a pronounced ring is present on which two pairs of bright spots and two pairs of less noticeable, tiny ones are situated. In each pair, the spots are located symmetrically with respect to the point $k_x = k_y = 0$, which indicates that the principal modes correspond to sets of intersecting convection rolls. They form cells, i.e., large-scale structures clearly distinguishable in the velocity–temperature field (Fig. 2). However, no signs of small-scale structures filling the entire domain and circulating inside the large-scale structures can be detected in the original spectrum.

We apply a two-dimensional band-pass filter to the flow pattern in order to select the components whose wavenumbers $[k]$ are in the range $2.5 < k < 7.5$ (Fig. 10). The resultant pattern testifies to the presence of two sorts of small-scale structures (Fig. 10a). This filtering procedure removes the long-wavelength

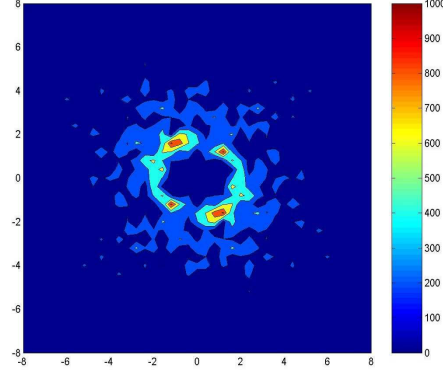


Figure 9. Flow spectrum (the k_x and k_y components of the wavevector \mathbf{k} are plotted on the axes) for $z = 0.97$.

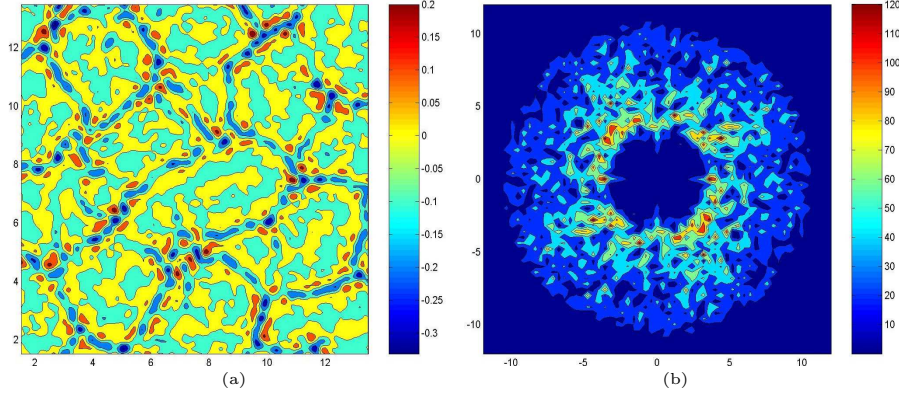


Figure 10. Processing of the temperature field with a band-pass filter for $z = 0.97$: (a) result of processing in physical space; (b) spectrum of the processed field.

component of the spectrum that corresponds to the ring $1.8 < k < 2$ (Fig. 9) and singles out the short-wavelength component (Fig. 10b). Inside the large (primary, or first-scale) structures, the smallest ones are advected by both the large-scale and intermediate-scale flows. The smallest structures are densely concentrated in the intercellular lanes of the primary structures, emerging near the borders of the intermediate-scale structures (Fig. 11). They are carried to the periphery of the larger structures along these very borders. In Fig. 10a, the smallest structures appear as blue and red mottles, which can be found not only near the borders of the primary structures but also in their centres.

A remarkable analogy between the spectrum of our simulated flow and that of solar convection should be noted. The flow has a continuous spectrum (Fig. 9), which declines with the wavenumber k , so that the modes corresponding to the second and third scales cannot be separated. A discrimination between the second and third scales in the spectrum of the processed pattern can also scarcely

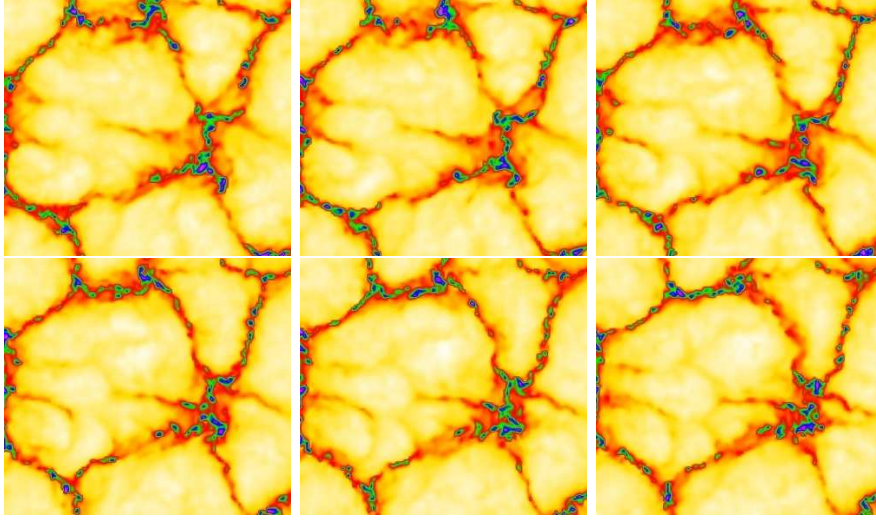


Figure 11. From left to right in the top and bottom rows: a fragment of the temperature field at times $t = 1.090, 1.096, 1.103, 1.110, 1.117, 1.123$ (measured in units of τ_ν). The largest, first-scale cells (outlined by downflow lanes shown in red) are divided by isthmuses into smaller, second-scale structures. The smallest, third-scale features (visible here as blue and green mottles) are concentrated in the network of first-scale intercellular lanes, especially at its nodes. The smallest features are advected by the flows inside the larger, first-scale and second-scale cells.

be made: we separated a spectral ring that corresponds to two smaller scales (Fig. 10b) but we failed to split it into two rings. Likely, this is because the second-scale and third-scale flow components, being most concentrated in the first-scale intercellular lanes, contribute to the main, first-scale spectral peak, becoming faint relative to the latter. The largest velocities and fluctuations of temperature correspond to the smallest-scale structures.

4. Summary and conclusion

We have analysed the structure of the velocity and temperature fields found in our simulation of the convection flow in a plane layer of fluid with temperature-dependent thermal diffusivity. This dependence is chosen so as to produce a sharp kink in the static temperature profile near the upper layer boundary. As a result, the magnitude of the (negative) static temperature gradient $[dT_s/dz]$ is small over the most part of the layer thickness but reaches large values in a thin boundary sublayer. The random temperature perturbation introduced in the strongly stratified sublayer initiates the development of convective motions, which are initially localised near the upper boundary and then penetrate into progressively deeper layers.

Shortly after the initiation of convection, within (dimensional) times $t \ll \tau_\nu$, the flow fills the whole layer depths, and the growing size of the largest structural elements of the velocity field – primary, or first-scale, convection cells – settles

down to a relatively steady characteristic value by $t \approx 0.16\tau_\nu$ (a well-developed multiscale convection pattern forms by $t \approx 0.26\tau_\nu$). The primary cells have central upflows and peripheral downflows. Although their vertical size corresponds to the layer thickness, not every cold sinking plume in the intercellular lanes apparently reaches the bottom layer boundary, since the high thermal conductivity smears the temperature differences between the plumes and the ambient fluid.

In contrast, smaller structural elements of the convective velocity field are localised near the upper boundary. We have identified second-scale structures, whose existence is evidenced by the presence of “bridges”, or “isthmuses”, intersecting the first-scale cells, and the smallest, third-scale structures, which are advected by the first-scale and second-scale convective flows. The third-scale structures are ubiquitous, they dot the horizontal sections of the layer located near its upper boundary and demonstrate a tendency to gather in the intercellular lanes of the first-scale cells.

Thus, the simulated convective flow is a superposition of cellular convection structures of three widely different characteristic sizes. This pattern bears remarkable similarities with the pattern of solar convection, which (apart from the existence of giant cells) is a superposition of three cell sorts, viz., supergranules, mesogranules and granules.

It is worth noting that the original spectrum of the flow does not directly indicate the presence of the second-scale and third-scale structures. In this respect, the situation resembles that in the case of solar convection: as we know, neither mesogranular nor mini-granular scale can be identified in the power spectra of the velocity field.

It is noteworthy that we managed to reveal the scale-splitting effect in the framework of a fairly simple model. The qualitative similarities between the simulated flow and the actually observed solar convection appear to be surprising. Hopefully, further improvements of the model would make this resemblance even more complete. We plan such attempts for the near future.

Acknowledgments We are grateful to V.V. Kolmychikov for developing the computational code for solving the Navier–Stokes equations and for his help in carrying out the computations. The work of O.V.Shch. and O.S.M. was supported by the Program “Leading Scientific Schools” (project no. NSh-9120.2016.2).

References

- Abramenko, V.I., Yurchyshyn, V.B., Goode, P.R., Kitiashvili, I.N., Kosovichev, A.G.: 2012, Detection of small-scale granular structures in the quiet Sun with the New Solar Telescope. *Astrophys. J. Lett.* **756**, L27. DOI. ADS.
- Beck, J.G., Duvall, T.L. Jr., Scherrer, P.H.: 1998, Long-lived giant cells detected at the surface of the Sun. *Nature* **394**, 653. DOI. ADS.
- Beck, J.G., Duvall, T.L. Jr., Scherrer, P.H., Hoeksema, J.T.: 1998, The detection of giant velocity cells on the Sun. In: S. Korzenik (ed.) *Structure and Dynamics of the Interior of the Sun and Sun-like Stars, ESA Special Publication* **418**, 725. ADS.
- Brummell, N., Cattaneo, F., Toomre, J.: 1995, Turbulent dynamics in the solar convection zone. *Science* **269**, 1370. DOI. ADS.

- Cattaneo, F., Lenz, D., Weiss, N.: 2001, On the origin of the solar mesogranulation. *Astrophys. J. Lett.* **563**, L91. DOI. ADS.
- Getling, A.V.: 1975, Convective motion concentration at the boundaries of a horizontal fluid layer with inhomogeneous unstable temperature gradient along the height. *Fluid Dyn.* **10**(5), 745. DOI. ADS.
- Getling, A.V.: 1980, Scales of convective flows in a horizontal layer with radiative transfer. *Izv., Atmos. Oceanic Phys.* **16**, 363. ADS.
- Getling, A.V.: 1998, *Rayleigh–Bénard Convection: Structures and Dynamics*, World Scientific; Russian version, Moscow: URSS, 1999, Singapore.
- Getling, A.V., Buchnev, A.A.: 2010, Some structural features of the convective-velocity field in the solar photosphere. *Astron. Rep.* **54**, 254. DOI. ADS.
- Getling, A.V., Tikhomolov, E.M.: 2007, Scale splitting in solar convection. In: *Trudy XI Pulkovskoi mezhdunarodnoi konferentsii po fizike Solntsa (Proc. 11th Pulkovo Int. Conf. on Solar Physics)*, 109.
- Getling, A.V., Mazhorova, O.S., Shcheritsa, O.V.: 2013, Concerning the multiscale structure of solar convection. *Geomagn. Aeron.* **53**, 904. DOI. ADS.
- Hathaway, D.H., Upton, L., Colegrove, O.: 2013, Giant Convection Cells Found on the Sun. *Science* **342**, 1217. DOI. ADS.
- Hathaway, D.H., Beck, J.G., Bogart, R.S., Bachmann, K.T., Khatrri, G., Petitto, J.M., Han, S., Raymond, J.: 2000, The photospheric convection spectrum. *Solar Phys.* **193**, 299. DOI. ADS.
- Kaczynski, T., Mischaikow, K., Mrozek, M.: 2003, *Computational Homology*, Springer, Berlin.
- Lawrence, J.K., Cadavid, A.C., Ruzmaikin, A.: 2001, Mesogranulation and turbulence in photospheric flows. *Solar Phys.* **202**, 27. DOI. ADS.
- Leighton, R.B., Noyes, R.W., Simon, G.W.: 1962, Velocity fields in the solar atmosphere. I. Preliminary report. *Astrophys. J.* **135**, 474. DOI. ADS.
- Mischaikow, K., Kokubu, H., Mrozek, M., Pilarczyk, P., Gedeon, T., Lessard, J.-P., Gameiro, M.: 2002, *Chomp: Computational homology project*, <http://chomp.rutgers.edu/>.
- Nordlund, Å., Stein, R.F., Asplund, M.: 2009, Solar surface convection. *Living Rev. Solar Phys.* **6**(2), 2, 1. DOI.
- November, L.J., Toomre, J., Gebbie, K.B., Simon, G.W.: 1981, The detection of mesogranulation on the Sun. *Astrophys. J. Lett.* **245**, L123. DOI. ADS.
- Rieutord, M., Rincon, F.: 2010, The sun’s supergranulation. *Living Rev. Solar Phys.* **7**(2), 2, 1.
- Schüssler, M.: 2013, Solar magneto-convection. In: Kosovichev, A.G., de Gouveia Dal Pino, E., Yan, Y. (eds.) *Solar and Astrophysical Dynamos and Magnetic Activity, Proc. IAU Symposium No. 294*, 95. DOI. ADS.
- Schüssler, M.: 2014, private communication
- Shcheritsa, O.V., Getling, A.V., Mazhorova, O.S.: 2015, Stratification-induced scale splitting in convection. *Adv. Space Res.* **55**, 927. DOI. ADS.
- Shine, R.A., Simon, G.W., Hurlburt, N.E.: 2000, Supergranule and mesogranule evolution. *Solar Phys.* **193**, 313. DOI. ADS.
- Simon, G.W., Leighton, R.B.: 1964, Velocity fields in the solar atmosphere. III. Large-scale motions, the chromospheric network, and magnetic fields. *Astrophys. J.* **140**, 1120. DOI. ADS.
- Simon, G.W., Brandt, P.N., November, L.J., Scharmer, G.B., Shine, R.A.: 1994, Large-scale photospheric motions: first results from an extraordinary eleven-hour granulation observation. In: R. J. Rutten & C. J. Schrijver (ed.) *Solar Surface Magnetism*, 261. ADS.
- Vögler, A., Shelyag, S., Schüssler, M., Cattaneo, F., Emonet, T., Linde, T.: 2005, Simulations of magneto-convection in the solar photosphere. Equations, methods, and results of the MURaM code. *Astron. Astrophys.* **429**, 335. DOI. ADS.